Understanding the Nature of the Kinetic Process in a VO_2 Metal-Insulator Transition

Tao Yao (姚涛),[1] Xiaodong Zhang (张晓东),[2] Zhihu Sun (孙治湖),[1] Shoujie Liu (柳守杰),[1] Yuanyuan Huang (黄元元),[1] Yi Xie (谢毅),[2,*] Changzheng Wu (吴长征),[2] Xun Yuan (袁勋),[3] Wenqing Zhang (张文清),[3] Ziyu Wu (吴自玉),[1,†] Guoqiang Pan (潘国强),[1] Fengchun Hu (胡凤春),[1] Lihui Wu (吴利徽),[1] Qinghua Liu (刘庆华),[1] and Shiqiang Wei (韦世强)[1,‡]

[1]*National Synchrotron Radiation Laboratory, University of Science and Technology of China, Hefei, Anhui 230029, People's Republic of China*

[2]*Department of Nanomaterials and Nanochemistry, Hefei National Laboratory for Physical Sciences at Microscale, University of Science and Technology of China, Hefei 230026, People's Republic of China*

[3]*State Key Laboratory of High Performance Ceramics and Superfine Microstructures, Shanghai Institute of Ceramics, Chinese Academy of Sciences, Shanghai 200050, People's Republic of China*

(Received 25 August 2010; published 23 November 2010)

Understanding the kinetics during the metal-insulator transition process is crucial to sort out the underlying physical nature of electron-lattice interactions in correlated materials. Here, based on the temperature-dependent *in situ* x-ray absorption fine structure measurement and density-functional theory calculations, we have revealed that the monoclinic-to-tetragonal phase transition of VO_2 near the critical temperature is characterized by a sharp decrease of the twisting angle δ of the nearest V–V coordination. The VO_2 metallization occurs in the intermediate monocliniclike structure with a large twist of V–V pairs when the δ angle is smaller than 1.4°. The correlation between structural kinetics and electronic structure points out that the structural rearrangement is a key factor to narrow the insulating band gap.

DOI: 10.1103/PhysRevLett.105.226405 PACS numbers: 71.30.+h, 61.05.cj, 71.27.+a

Complex transition-metal oxides have attracted widespread attention owing to the special phenomena of unconventional electronic and magnetic phase transitions [1,2]. However, understanding the nature of metal-insulator transitions (MITs) in correlated materials remains challenging [3–5]. Vanadium oxide (VO_2) can be considered as an archetypical MIT system with a conductivity change of several orders at the critical temperature T_C (341.1 K), accompanied by a transition in lattice structure from a monoclinic to a tetragonal phase and a dramatic increase of the infrared absorbance [6–8]. Although various techniques, including spatial- and time-resolved probes and x-ray absorption fine structure (XAFS) spectroscopy have been applied to investigate this transition [5,9–13], the underlying physics of MITs in VO_2 is still an open question. An electron-correlation-driven Mott transition [5,11], a structure-driven Peierls transition [14,15], or the cooperation of these two mechanisms [12,13] have been proposed. The controversy is mainly due to the lack of a bridge between atomic and electronic kinetics during the MIT process of VO_2. Several recent studies have addressed interesting aspects of this system and pointed out the formation of a metallic domainlike state in the monoclinic VO_2 near MITs [5,11,16]. Apparently, the tetragonal lattice structure is not necessary to the appearance of a metallic behavior in VO_2, in agreement with the hypothesis of a Mott transition. However, important questions arise: What is the precise structure of the intermediate states, and do structural variations and MITs occur simultaneously? How does the tetragonal phase evolve from the monoclinic phase, and what is the key parameter controlling the structural evolution? Some hints could be associated with the fact that the nearest V–V coordination, which plays a critical role in determining the electronic properties of VO_2, undergoes a significant ''depairing'' across the MIT [15]. So far, most of the published works are focused on the features of the initial and final states of the MIT process and provide relatively scarce information on the structural evolutions near T_C. In order to address the above issues, an accurate *in situ* investigation of the kinetic process of the monoclinic-to-tetragonal phase evolution would clarify the interplay between atomic rearrangements and electronic structure changes of the whole VO_2 MIT process.

In this work, using the temperature-dependent *in situ* XAFS technique, we detect the atomic kinetics across the MIT in crystalline VO_2 during a heating-cooling cycle. Since the atomic and electronic structures of VO_2 change significantly in a narrow temperature range around T_C, this characterization technique is sensitive in monitoring the structural evolution across T_C. The experimental setup including the high precision temperature controller enables us to control temperature variations of ± 0.2 K [Fig. 1(a)]. Compared to ultrafast pulse-induced transitions, a thermally driven transition is slow. It may keep the VO_2 system in a stable intermediate state, allowing the determination of accurate spatial positions near T_C. The VO_2 was prepared by the annealing method [17], a standard and reliable way to obtain monoclinic VO_2 with high crystallinity [18]. The phase homogeneity and the reversible transition characteristics were confirmed by differential scanning calorimetry

and x-ray diffraction (XRD) (Figs. S1 and S2 in Ref. [17]) measurements. Temperature-dependent *in situ* XAFS data (V *K* edge) at a series of temperatures were recorded in transmission mode at U7B and U7C stations of the National Synchrotron Radiation Laboratory, China.

Figures 1(b) and 1(c) show V *K*-edge *in situ* XAFS spectra of crystalline VO_2 within the temperature range 298–350 K. In about 3° around T_C, the extended XAFS (EXAFS) functions $\chi(k)$ and Fourier transforms exhibit remarkable and systematic evolutions. The $\chi(k)$ oscillation shape of the monoclinic VO_2 is significantly different from that of the tetragonal one in the k range 4–8 $Å^{-1}$ as shown in the yellow-hatched region in Fig. 1(b). Correlated changes can be identified in the Fourier transform profiles in the real space [Fig. 1(c)]. The Fourier transform curves in the monoclinic phase region are characterized by four distinct peaks: two peaks at 1.20 and 1.63 Å corresponding to the chemical bonds of the V–O split, and the other two at 2.12 and 2.86 Å associated to V–V1 and V–V2 bonds, respectively. By increasing the temperature to 339.8 K, the intensity of the first peak at 1.20 Å decreases significantly, while the second peak grows in intensity and moves to 1.55 Å. At the temperature of 343 K and above, the two V–O split peaks merge in a single peak at 1.48 Å, indicating an increased symmetry of the [VO_6] octahedral geometry with comparable V–O bond lengths for the tetragonal phase [14]. Moreover, the V–V1 peak at 2.12 Å shifts to 2.36 Å, which can be explained as a change of the dimerization of the V–V pairs at a distance of 2.65 Å in the monoclinic phase to the elongated distance 2.85 Å in the tetragonal phase. To our knowledge, this is the first *in situ* temperature-dependent XAFS study of the transition of the VO_2 structural kinetic phase from the initial monoclinic to the final tetragonal phase.

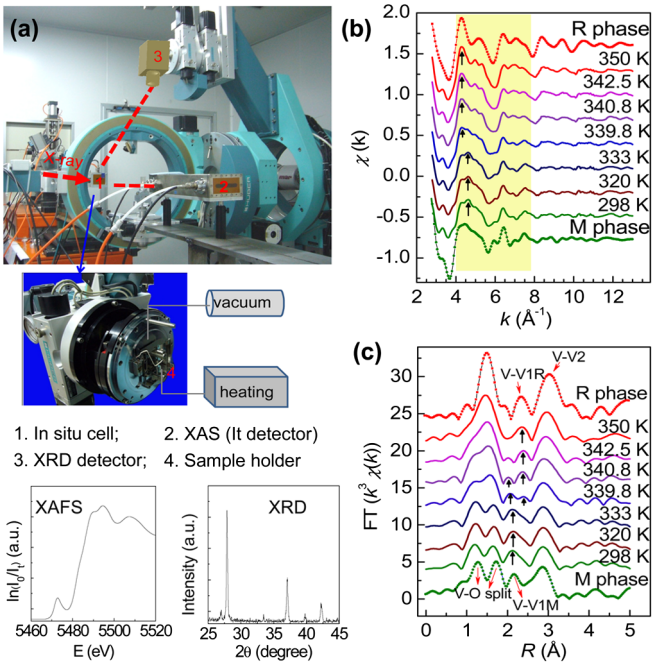

FIG. 1 (color online). (a) The experimental setup of the temperature-dependent *in situ* XAFS and XRD. V *K*-edge EXAFS oscillations [$\chi(k)$] (b) and their Fourier transforms (c) at several temperatures during the heating process.

To obtain quantitative structural information during the VO_2 MIT, a least-squares parameter fitting using the ARTEMIS module [19] of IFEFFIT was performed [17]. The V–O and V–V distances among all the best fit parameters (Table S1 in Ref. [17]) are shown in Fig. 2(a). The fitting results point out that, when moving from a monoclinic to a tetragonal phase, the VO_2 structure shows an increased symmetry both in the [VO_6] octahedron and in the V atomic chains, as manifested by the overlap of V–O and V–V peaks. In this process, the V–V pairs in the chains undergo not only the elongation of V–V1a and the shortening of V–V1b but also a twist from the zigzag-type to a linear chain. To determine this critical angle, based on the structural characteristic and similarities between the monoclinic and tetragonal phases, we show in Fig. 2(b) the supercell structure of both VO_2 phases. It can be clearly seen that V atoms dimerize and the V–V pairs tilt around the a_M axis for the monoclinic phase (the direction of V atoms marked by black arrows). The twist of V–V pairs can be quantitatively characterized by the angle δ defined as

$$\delta = \arccos\frac{(\frac{1}{2}R_{\mathrm{V-V1}a})^2 + (\frac{1}{2}a_M)^2 - (\frac{1}{2}R_{\mathrm{V-V1}b})^2}{2 \times \frac{1}{2}R_{\mathrm{V-V1}a} \times \frac{1}{2}a_M},$$

where $R_{\mathrm{V-V1}a}$, $R_{\mathrm{V-V1}b}$, and a_M values can be obtained via a structural fit (Table S2 in Ref. [17]). Combining the above results, we reconstruct the crystal structure variations at the atomic level in Fig. 3 and Fig. S4 in Ref. [17].

To understand the nature of the MIT, we compare the temperature dependence of the twisting angle δ [Fig. 4(a)] with the resistance [Fig. 4(b)] behavior of the crystalline VO_2. In Fig. 4(a), the graph of δ vs temperature shows a well-defined hysteresis loops. In the two-dimensional

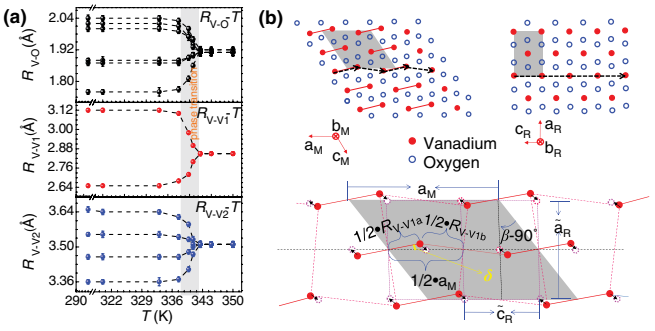

FIG. 2 (color online). (a) Temperature profiles of the bond distances as obtained by the EXAFS fit. (b) The top panel presents the microscopic structures of monoclinic and rutile VO_2 projected along [010]. The distortion of V atoms is outlined by black arrows along the *a* axis (*c* axis for the rutile cell). The bottom panel shows the motions of V atoms and the correlations among unit cell parameters between two phases. δ is the twisting angle of the V–V pairs.

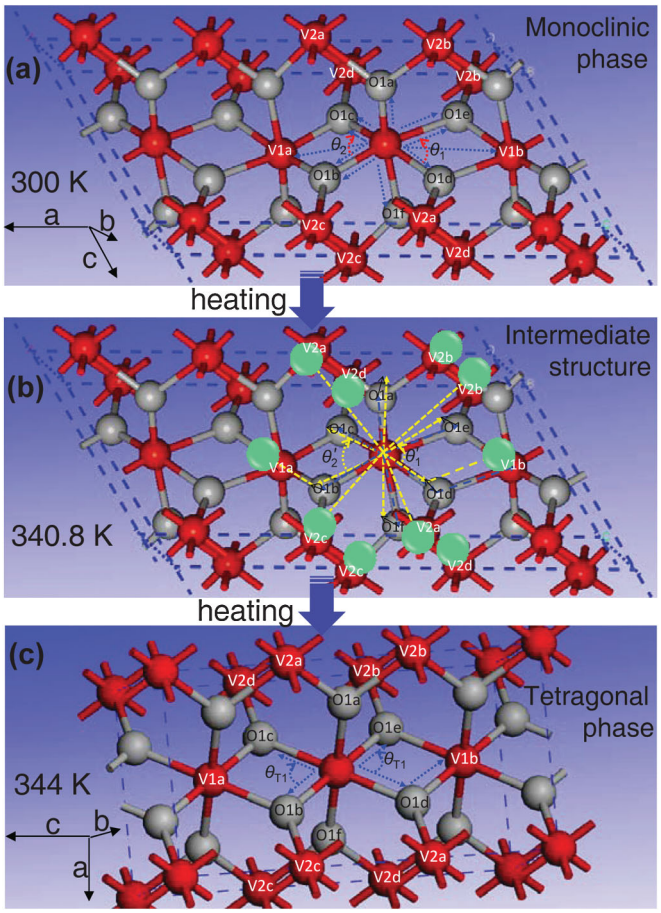

FIG. 3 (color). (a) The initial monoclinic phase, (b) the intermediate structure during the heating process, and (c) the final tetragonal phase. The θ_{T1} in the tetragonal phase evolve from the θ_1 and θ_2 angles of the monoclinic phase. For the sake of simplicity, the V atom is fixed relatively to the adjacent O and V atoms.

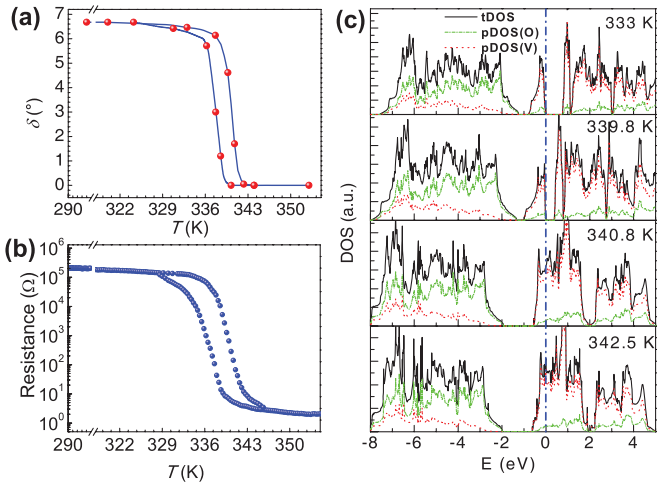

FIG. 4 (color online). (a) Plot of the twisting angle δ vs temperature and (b) the temperature dependence of the resistance during the thermal cycle of heating and cooling. (c) DOS of the intermediate VO_2 structure at different temperatures calculated by using the density-functional theory method.

space, the twisting angle δ may well characterize in a quantitative way the VO_2 phase transition. Starting from an initial value of about 7°, it drops abruptly to zero in the range 338–341 K. The resistance shows a drop of 4 orders of magnitude within 5° (338–343 K) during the heating process. The similar hysteretic behavior of δ, in both the temperature range and the transition point, confirms the high quality of the samples [20] and suggests a strong dependence of the electronic behavior to structural changes (i.e., the twisting angle δ). This implies that the change of the electronic property and the structural phase transition occur simultaneously, suggesting for the MIT of VO_2 a cooperative mechanism of a structurally driven (Peierls) mechanism and the electron correlation (Mott).

To confirm this interpretation, we also performed density-functional theory calculations based on the atomic structural parameters by *in situ* XAFS. The obtained densities of states (DOS) for the series of transitional VO_2 structures at several different temperatures are shown in Fig. 4(c). For the insulator phase, the Fermi level is generally selected as the position of the highest occupied state in the valence band, while the position of the Fermi level in a metallic system is determined by the number of itinerant electrons. The calculated band gap for the monoclinic phase at RT is about 0.6 eV, in agreement with experimental results by photoemission spectroscopy [13] and calculations based on the cluster dynamical mean field theory [21]. The gap of the VO_2 intermediate structure at 339.8 K gradually narrows to 0.36 eV. For the intermediate structure at 340.8 K, the gap becomes zero, revealing a metallic-like behavior, consistent with the large drop of the resistance (about 4 orders of magnitude) as compared with the initial insulating phase.

It should be underlined here that the tetragonal phase is associated to a high symmetry characterized by the angle $\delta = 0°$, and data show that the lattice structure leaves the asymmetric monoclinic configuration only when the full transition in the tetragonal phase occurs [see Fig. 2(b)]. As an example, at 340.8 K, the intermediate state characterized by the angle δ of about 1.4° still belongs to the monoclinic phase. Hence, we propose that in crystalline VO_2 the metallic phase is formed before a full transformation to the tetragonal phase. The claim is in agreement with a recent micro-XRD investigation on a VO_2 film showing that a metallic behavior appears at the applied voltage of 4 V while diffraction plane characteristics of the tetragonal structure are observed only when the voltage increases to about 7 V [22]. In this work, however, we show that increasing the temperature induces a reduction of δ from 7° to 1.4° and a local structure distortion from the normal monoclinic phase to a new metallic monoclinic phase. A similar phenomenon has been reported in the pressure-induced metallization process in VO_2 [23]. Although the metallic phase exists without the full transformation into the VO_2 tetragonal structure, it can be speculated that the rearrangement of the *V* chains within the monoclinic

lattice play an important role in inducing this phenomenon, which means that the changes of atomic and electronic structures occur simultaneously. Taking into account the pure monoclinic phase for the initial sample at RT and a vacuum *in situ* cell (10^{-6} Pa) used in XAFS measurements, the VO_2 phase transition could be regarded as a continuous (homogenous) process from the initial monoclinic to the final tetragonal phase with a series of intermediate structures. No other tetragonal or monoclinic phase coexists in this process within the detection limit of XAFS.

We explain this scenario in the framework of the molecular-orbital picture [15,21]. The dimerization and the off-axis zigzag displacement of V–V pairs induce a splitting of the a_{1g} band and the high shifting of the e_g^{π} band, forming a Peierls-like gap at the Fermi level. The band gap is thus determined by the localized charge variation, which depends on changes in V–V pair twist and varies sensitively with the separation of V–V pairs along the c axis. Quantitatively, the semiempirical expression for the separation of V $3d$ electrons reveals that, when the V–V distance is reduced to the critical distance (2.94 Å), the coupling interaction between $3d$ electrons leads to the itinerant electronic behavior. In the monoclinic VO_2, the dimerization and tilt of V–V pairs give rise to alternating short V–V1a (2.65 Å) and long V–V1b (3.12 Å) distances. Actually, the value of long V–V1b is significantly larger than the critical distance, and thus the d-orbit electrons are localized within the short V–V pairs, leading to the insulator behavior. However, at 340.8 K, the fit shows a $R_{\mathrm{V-V1}b}$ value of 2.90 Å smaller than the critical distance, a condition that makes possible a delocalization of the d electrons among all V atoms to give the metallic behavior of VO_2. The observed metallic behavior in the structure within the monoclinic framework is due to the change of 0.2 Å of the V–V distance, which implies the role of the correlation in the transition. In view of the concurrent evolutions of the atomic and the electronic structure as well as the presence of an intermediate monocliniclike structure with a metallic character, we consider that both the structural distortion induced by temperature and the electron correlations are active and contribute to the MIT in VO_2 near T_C.

Using temperature-dependent *in situ* XAFS spectroscopy combined with density-functional theory calculations, we have been able to resolve fine changes in the atomic and electronic kinetics of VO_2 across the MIT with high accuracy. The structural phase transition can be definitely characterized by the twisting angle δ. A continuous series of intermediate structures have been configured, in which the variation of nearest V–V pairs is found to play a key role on the evolutions of the electronic structures, leading to the formation of the transitional structure with the monoclinic symmetry exhibiting the metallic behavior. The strong correlation among atomic spatial rearrangements, electronic structures, and electrical resistance supports a cooperative mechanism for the VO_2 MIT. These results establish a clear correlation between the dynamics of the lattice structure and electronic properties and clarify a possible structural pathway and the mechanism of similar phase transitions in correlated materials.

This work is financially supported by the National Basic Research Program of China (No. 2009CB939901), the National Natural Science Foundation of China (No. 10725522, No. 11079004, No. 10635060, No. 10979047, and No. 90922016), the Knowledge innovation project of the Chinese Academy of Sciences (KJCX2-YW-N40 and KJCX2-YW-H2O), and Shanghai Key Basic Research Project (3109DJ1400201).

*Corresponding author.
yxie@ustc.edu.cn
†Corresponding author.
wuzy@ustc.edu.cn
‡Corresponding author.
sqwei@ustc.edu.cn

[1] Y. Tokura and N. Nagaosa, Science **288**, 462 (2000).
[2] T. Driscoll *et al.*, Science **325**, 1518 (2009).
[3] M. Imada, A. Fujimori, and Y. Tokura, Rev. Mod. Phys. **70**, 1039 (1998).
[4] P. Baum, D. S. Yang, and A. H. Zewail, Science **318**, 788 (2007).
[5] M. M. Qazilbash *et al.*, Science **318**, 1750 (2007).
[6] F. J. Morin, Phys. Rev. Lett. **3**, 34 (1959).
[7] L. Whittaker *et al.*, J. Am. Chem. Soc. **131**, 8884 (2009).
[8] C. Z. Wu *et al.*, Adv. Mater. **22**, 1972 (2010).
[9] J. Cao *et al.*, Nature Nanotech. **4**, 732 (2009).
[10] C. Kubler *et al.*, Phys. Rev. Lett. **99**, 116401 (2007).
[11] H. T. Kim *et al.*, Phys. Rev. Lett. **97**, 266401 (2006).
[12] M. W. Haverkort *et al.*, Phys. Rev. Lett. **95**, 196404 (2005).
[13] T. C. Koethe *et al.*, Phys. Rev. Lett. **97**, 116402 (2006).
[14] J. M. Booth and P. S. Casey, Phys. Rev. Lett. **103**, 086402 (2009).
[15] J. B. Goodenough, J. Solid State Chem. **3**, 490 (1971).
[16] J. G. Ramirez *et al.*, Phys. Rev. B **79**, 235110 (2009).
[17] See supporting material at http://link.aps.org/supplemental/10.1103/PhysRevLett.105.226405 for detailed information on the experimental and calculated process, differential scanning calorimetry, x-ray diffraction, and EXAFS parameters.
[18] C. Z. Wu *et al.*, Angew. Chem. **122**, 138 (2010).
[19] B. Ravel and M. Newville, J. Synchrotron Radiat. **12**, 537 (2005).
[20] D. H. Kim and H. S. Kwok, Appl. Phys. Lett. **65**, 3188 (1994).
[21] S. Biermann *et al.*, Phys. Rev. Lett. **94**, 026404 (2005).
[22] B. J. Kim *et al.*, Phys. Rev. B **77**, 235401 (2008).
[23] E. Arcangeletti *et al.*, Phys. Rev. Lett. **98**, 196406 (2007).